Nanopit-induced osteoprogenitor cell differentiation: The effect of nanopit depth

Martin J Davison, Rebecca J McMurray, Carol-Anne Smith, Matthew J Dalby and RM Dominic Meek

Abstract

We aimed to assess osteogenesis in osteoprogenitor cells by nanopits and to assess optimal feature depth. Topographies of depth 80, 220 and 333 nm were embossed onto polycaprolactone discs. Bone marrow–derived mesenchymal stromal cells were seeded onto polycaprolactone discs, suspended in media and incubated. Samples were fixed after 3 and 28 days. Cells were stained for the adhesion molecule vinculin and the osteogenic transcription factor RUNX2 after 3 days. Adhesion was lowest on planar controls and it was the shallowest, and 80-nm-deep pits supported optimal adhesion formation. Deep pits (80 and 220 nm) induced most RUNX2 accumulation. After 28 days, osteocalcin and osteopontin expression were used as markers of osteoblastic differentiation. Deep pits (220 nm) produced cells with the highest concentrations of osteopontin and osteocalcin. All topographies induced higher expression levels than controls. We demonstrated stimulation of osteogenesis in a heterogeneous population of mesenchymal stromal cells. All nanopit depths gave promising results with an optimum depth of 220 nm after 28 days. Nanoscale modification of implant surfaces could optimise fracture union or osteointegration.

Keywords

Osteointegration, nanotopography, osteoprogenitor

Received: 29 March 2016; accepted: 9 May 2016

Introduction

The control and modification of surfaces on a micro and nanoscale has been shown to affect cell interaction with the material. Adherence,[1–7] metabolic activation,[4,8] alignment,[9] gene expression[1,10–12] and differentiation[2,7,11,13] can all be controlled by topographical cues detected by the cells in contact with the surface. Osteoprogenitor cells and selected mesenchymal stem cells have been shown to respond to certain topographical patterns by preferentially differentiating into mature osteoblasts and exhibit higher levels of osteogenesis compared with planar control substrates. Furthermore, levels of osteogenic differentiation in response to topographic features alone have been observed to be similar to those using osteogenic differentiation supplements.[2,14]

In orthopaedic surgery, osteogenesis is key to fracture healing and osteointegration of implanted material. In uncemented arthroplasty implants, such as acetabular components of hip replacements, a stable implant with bony ingrowth correlates with longer implant survivorship and better function.[15] Commonly, however, the implant–bone interface can produce a host response that results in fibrous encapsulation of the foreign material leading to early loosening and a threefold increase in pain.[15] Because topography does not rely on changes in chemistry

Centre for Cell Engineering, Institute of Molecular, Cell and Systems Biology, College of Medical, Veterinary and Life Sciences, University of Glasgow, Glasgow, UK

Corresponding author:
Martin J Davison, Centre for Cell Engineering, Institute of Molecular, Cell and Systems Biology, College of Medical, Veterinary and Life Sciences, University of Glasgow, Joseph Black Building, Glasgow G12 8QQ, UK.
Email: martindavison@doctors.net.uk

and substrate mechanical properties, micro/nanoscale modification of the implant surface is a potential strategy for future implants to encourage a shift towards osteointegration preferentially instead of fibrosis.

A previous report has suggested that diameters of 30 μm are strongly osteogenic through mimicry of topographic features such as those left by osteoclasts in resorption pits.[7] This ties in with previous observations of 40-μm-diameter pits being osteogenic.[10,16] However, in these reports, linking feature depth to osteogenesis was largely unexplored and cell lines rather than primary cells were mainly used. Thus, here, we use a heterogeneous bone marrow–derived mesenchymal stromal cell mix which is present around an uncemented arthroplasty component inserted into cancellous bone. Furthermore, we fix diameter at 30 μm and focus on assessment of nanopit depth (ranging from 80 to 333 nm) and osteoinductive potential.

In order to achieve this, we first study cell adhesion to the features. Cell adhesion and derived intracellular tension is key to osteogenesis. Mesenchymal stem cells and osteoblasts actively expressing bone markers (differentiating) use large, stable adhesions, many of which are greater than 5 μm in length and which are termed super-mature adhesions.[1,17] Adhesion allows anchoring of the actin cytoskeleton and activation of the G-protein Rho, responsible for promoting actin/myosin regulated cytoskeletal contraction. This tension, mediated through Rho A kinase (ROCK), promotes osteogenesis as has been evidenced through mesenchymal stem cell interactions with substrates that have been chemically, mechanically and topographically modified.[13,18–22]

Such changes in adhesion and cytoskeletal signalling will lead to changes in key signalling hubs such as extracellular signal–related kinase (ERK1/2). ERK1/2 is central to cell growth. However, increases in integrin signalling (e.g. from formation of super-mature adhesions) drive negative feedback on ERK1/2 and phosphorylation of the osteogenic transcription factor runt-related transcription factor 2 (RUNX2).[23–25] RUNX2 activation allows for transcription of major osteoblast associated genes such as osteocalcin (OC).[26] Hence, we study expression of RUNX2, OC and osteopontin (OPN) as indicators of the cells forming an osteoblast phenotype on the materials.

Materials and methods

Fabrication

Polycaprolactone (PCL) discs (Aldrich, average Mn 45,000) with the specific surface topographies (all 30 μm diameter, with a depth of 80, 220 or 333 nm) were created using the nickel shims and a hot embossing technique at 80°C (see Supplementary Information). Discs were trimmed to 1 cm diameter. Samples embossed with each topography, as well a control samples melted on a planar surface, were examined by scanning electron microscopy (SEM) to validate the technique. Samples were treated with three 10-s 70% ethanol emersions followed by serial emersions in HEPES saline prior to use.

Cell culture

Ethical approval for use of discarded human tissue was in place through NHS Greater Glasgow and Clyde. After obtaining informed consent, a bone aspirate was obtained from the femoral neck of a healthy adult at the time of total hip replacement for osteoarthritis. Samples obtained in this manner have been shown to contain a mixed cell population of osteoprogenitor cells,[27] ranging from mesenchymal stem cells to mature osteoblasts. A total of 10 mL of aspirate was added to transfer media (10 mL phosphate-buffered saline (PBS), 0.03 g EDTA sterilised in autoclave). This was then washed with basal media (Dulbecco's modified Eagle's medium (DMEM), 10% foetal bovine serum, sodium pyruvate and non-essential amino acids) and centrifuged at 300g for 6 min.

This cell population was isolated from contaminating erythrocytes and plasma by Ficoll-Paque medium. Cells were cultured in basal media at 37°C and media were changed twice weekly. After two passages, and once samples were 90% confluent, cells were seeded onto the PCL discs containing the topographies at a density of 1×10^4 cells in 1 mL of basal media in 24 well flasks. A total of 12 identical wells were prepared for each topography and control, to allow each of the four markers to be stained in triplicate. Again, all samples were incubated at 37°C and media changed twice weekly.

Immunofluorescence

After 3 days, half of the samples were fixed using 4% formaldehyde/PBS, with 1% sucrose at 37°C for 15 min. When fixed, the samples were washed with PBS and a permeabilising buffer (10.3 g sucrose, 0.292 g NaCl, 0.06 g MgCl$_2$, 0.476 g HEPES buffer, 0.5 mL Triton X, in 100 mL water, pH 7.2) added at 4°C for 5 min. Samples had anti-vinculin (1:150 in 1% bovine serum albumin (BSA)/PBS, Sigma, UK), rhodamine-conjugated Phalloidin (1:50% BSA/PBS, Invitrogen, UK), or anti-RUNX2 (raised in rabbit, Insight Biotechnology, UK) added for 1 h at 37°C. Samples were then washed with 0.5% Tween 20/PBS (5 min × 3). Secondary biotin-conjugated antibodies (either anti-rabbit or anti-mouse, 1:50 in 1% BSA/PBS, Vector Laboratories, UK) were added for 1 h at 37°C prior to washing. The tertiary, fluorescein isothiocyanate (FITC)-conjugated streptavidin, layer was then added (1:50 in 1% BSA/PBS, Vector Laboratories) and samples incubated at 4°C for 30 min. Discs, with fixed and stained cells on their surface, were then mounted on slides with Vectorshield mounting medium with

4',6-diamidino-2-phenylindole (DAPI) (Vector Laboratories). After 28 days, the remaining live samples were fixed and stained for either OPN or OC (both 1:150 raised in mouse, Insight Biotechnology, UK) using the above protocol. Samples were viewed under fluorescence microscope (Zeiss Axiovert 200M – 10–40× magnification, NA 0.5). Images were analysed using Photoshop CS (Adobe) and ImageJ, analysing 40 individual cells in each group for staining intensity and morphology.

Results

Materials

SEM of the PCL discs showed successful embossing of the topographies with a consistent 30 µm pit diameter with 90 µm centre–centre pit spacing in all samples in a square arrangement. Planar controls lacked any significant irregularities or patterning and were essentially smooth (Figure 1).

Cytoskeleton and morphology

After 3 days, the cells were seen to be well spread on all surfaces with well developed, abundant actin stress fibres (Figure 2). The stress fibres were particularly noteworthy on the 80-nm-deep pitted samples.

Cell adhesions

Vinculin expression was assessed after 3 days of culture. Individual cells, which had no identifiable contact with other cells, were selected for analysis to eliminate the influence of 'cell to cell' interaction instead of 'cell to surface' adhesion. A total of 40 cells in each group were analysed. Lower concentrations of vinculin were seen around the periphery of cells in the planar control group. Cells on the shallowest pits, 80 nm, had the highest levels of vinculin expression with notably larger and more distinct adhesions. However, it is noted that all the pitted surfaces supported more mature adhesions than the planar control (Figure 2).

Early osteoblastic differentiation

Expression of RUNX2, a transcription factor involved in osteoblastic differentiation, was assessed after 3 days. The data show that while RUNX2 could be noted in the nuclei of cells on the planar surface, more intense nuclear staining and also cytoplasmic staining of the transcription factor was noted in cells on the topographies, particularly the 80- and 220-nm-deep pits (Figure 2).

Expression of osteoblast phenotype

OC and OPN expression after 28 days were used as markers of cell differentiation into an osteoblastic
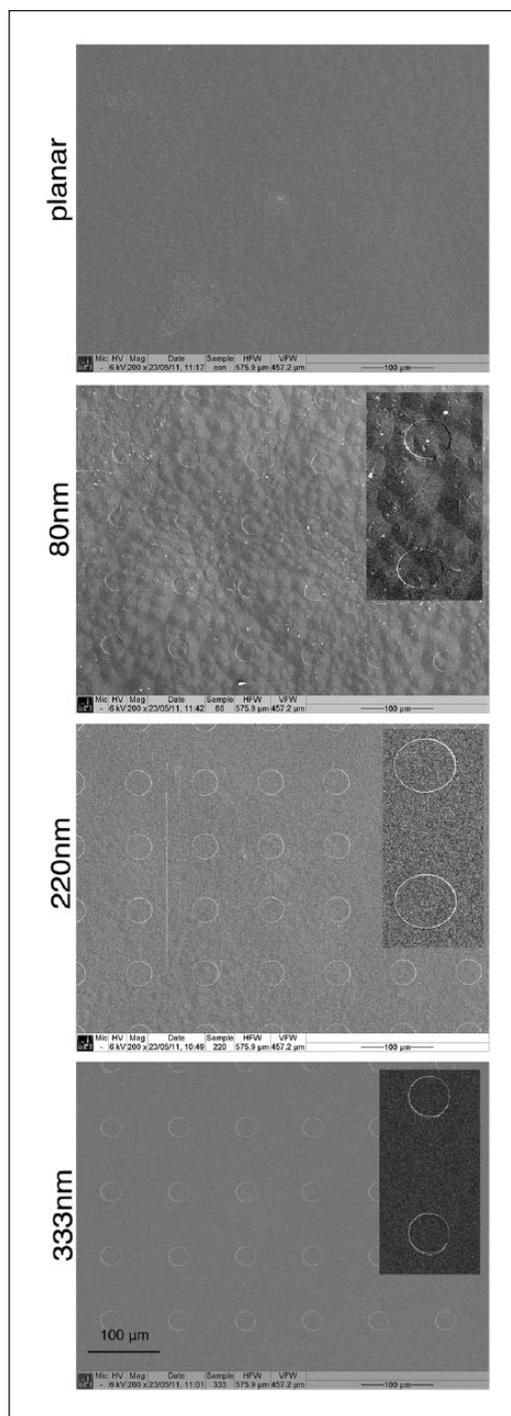

Figure 1. SEM of embossed nanopits on polycaprolactone showing successful imprinting compared with the planar controls which were effectively flat.

phenotype. Using microscopy, cell populations were found to be well established on all surfaces and controls with large aggregates of cells spread through the discs. OPN in particular showed high levels of cytoplasmic and extracellular staining on topographies compared with planar controls (Figure 3).
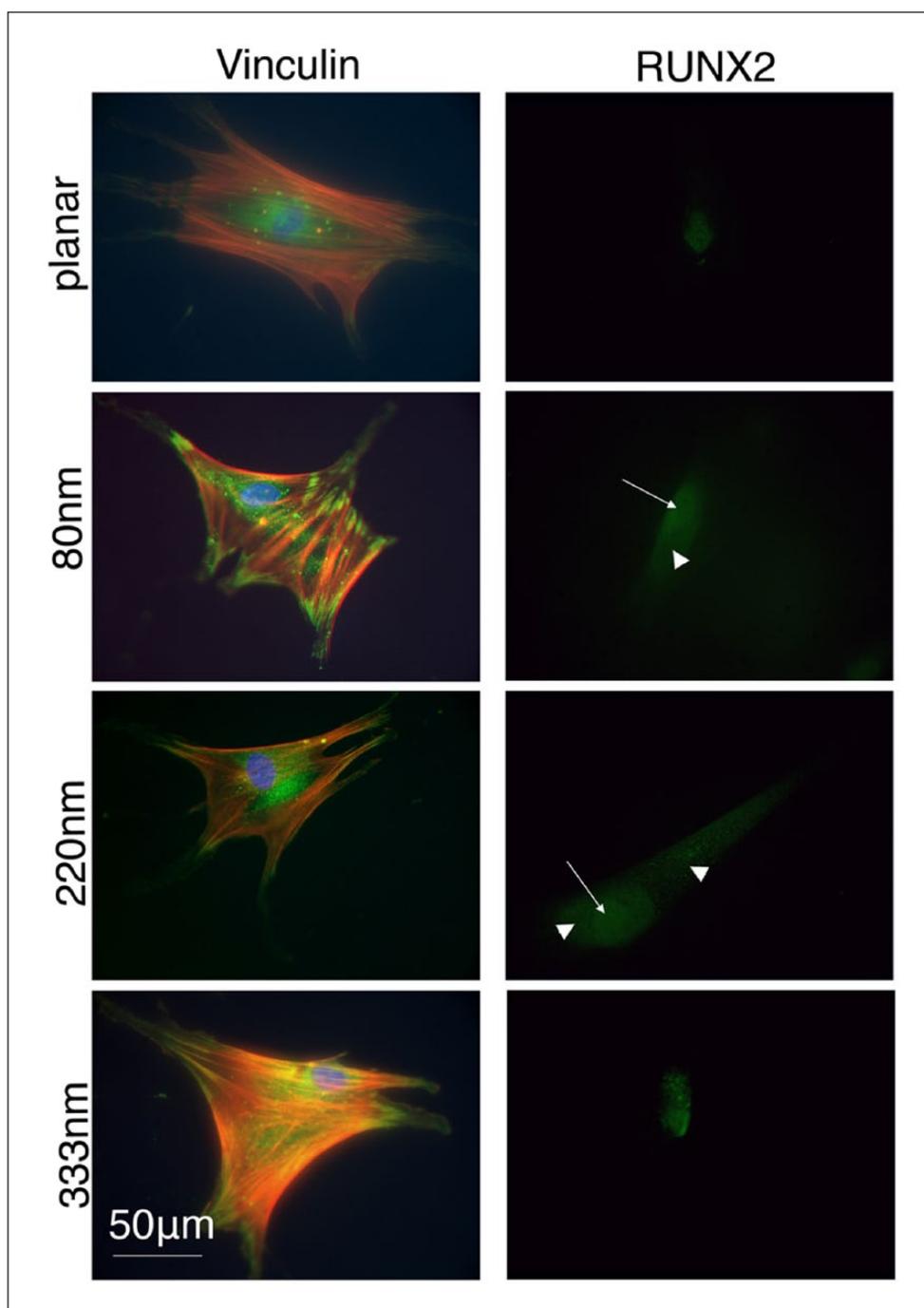
Figure 2. Cells fixed after 3 days showing actin (cytoskeleton), vinculin (adhesion) and RUNX2 (osteoblastic transcription factor) staining. Vinculin formed large, distinct adhesion complexes at the peripheries of cells particularly on the 80-nm-deep features and the other topographies compared to control. Concomitantly, actin stress fibres were also more organised. RUNX2 had increased nuclear and cytoplasmic concentrations on the topographies compared with controls (arrows indicate nuclear localisation and arrowheads indicate cytoplasmic localisation).

Cells cultured on the 220-nm-deep pits were consistently observed to contain the highest concentrations of OPN. In contrast, only a perinuclear blush of OPN staining was visible on control samples, even when using high contrast settings. Using ImageJ analysis, multiple slides consistently showed higher staining intensity for 220-nm-deep pits compared with controls or other topographies. Average OPN staining intensity per slide for 220 nm pits was compared to control, 80 nm and 333 nm pits using Student's t-tests ($p = 0.017$, 0.029 and 0.045, respectively). Mean staining intensity of OPN per cell was also calculated for all images captured to control the variable of cell density
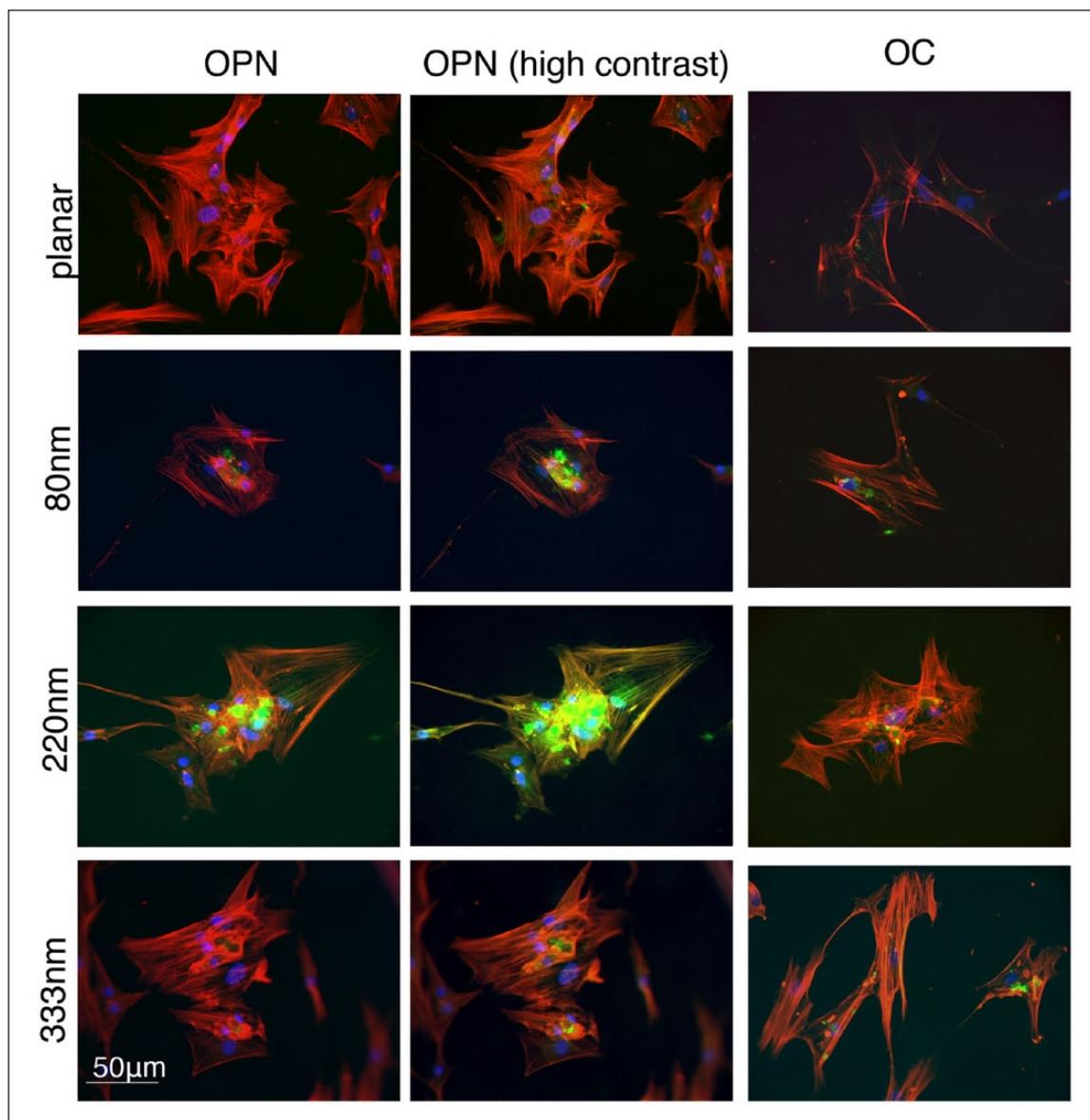
Figure 3. Cells fixed after 28 days showing osteopontin (OPN) and osteocalcin (OC) expression, representing differentiation and maturation of cells into an osteoblastic phenotype. Only background staining and a perinuclear blush of OPN were present on planar controls. Using identical high contrast settings, the difference in OPN staining becomes more apparent. Consistently higher levels of both markers were seen in cells on the pits, especially on the 220-nm-deep pits.

when comparing different slides (Figure 4). Increased levels of OPN were again observed with 220-nm-deep topographies. Staining intensity of OC after 28 days also suggested superior osteoblastic differentiation on 220-nm-deep pits (Figure 3). The other topographies, 80 and 333 nm, also showed a trend towards increased OPN and OC expression compared to controls, but this did not reach statistical significance.

Discussion

Honing of surface nanopatterning to optimise and steer targeted cell response is dependent on a number of factors.

Size, shape, spacing and configuration of the nanostructures (islands, grooves or pits) as well as the material's physicochemical properties play an important role. The chemical properties of the surface have been shown to have an independent influence on osteoblast activation compared with topographic modification.[28] A limiting factor can be the feasibility and reproducibility of nanofabrication in the chosen material.

In terms of osteogenesis, cells of an osteoblastic lineage must be stimulated to adhere, undergo preferential differentiation and metabolic activation with the final desired outcome of osteoid matrix synthesis and deposition. Adherence can initiate a cascade of intracellular
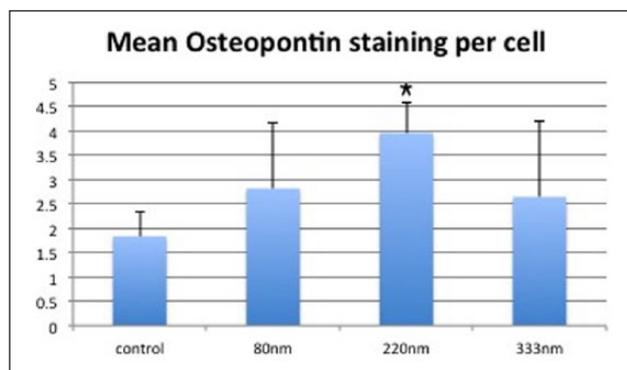
Figure 4. Graph showing mean staining intensity of osteopontin after 28 days to correct for variable cell density between slides. Staining intensity was calculated 'per cell' using all images captured at 20× magnification. Y-axis: arbitrary units of staining intensity. 220- and 333-nm-deep pits performed best with the planar controls consistently showing the lowest levels of staining. Results = mean ± SD, *$p < 0.05$ compared to planar control by Student's *t*-test.

signalling and essentially acts to transfer information from the physical environment to make the cell 'spatially aware'. Several theories are being explored to explain the exact nature of the topography–cell interaction.[29] Adhesion formation and filipodia play part in contact guidance as part of this process.

It is perhaps not such a large surprise that shallower pits, 80 and 220 nm, showed superior adhesion and osteogenic induction than the deeper pits (333 nm). Osteoblasts have been shown to interact with nanogrooves with a depth of only 17 nm.[12] Human foetal osteoblasts have been shown to exhibit superior adhesion formation on 14- and 29-nm-deep pits compared with 45-nm-deep pits.[30] In terms of the smallest topographical features, the threshold for contact guidance of fibroblasts to occur has been shown to be 35 nm.[31] Even smaller features, for example, 15 nm titanium nanopillar structures, had been shown to have the most osteoinductive potential compared with larger features[4] and Mesenchymal stem cells (MSCs) have been shown to interact with features just 8 nm high.[32] All these suggest that all features used in this study are of a size that can potentially interact and guide contacting cells.

On day 3, increased adhesion sizes and levels of cytoskeletal organisation could be noted on the features, particularly the 80-nm-deep pits. This is important in osteogenesis as recruitment of focal adhesion kinase (FAK) and activation of G-proteins is considered key to osteogenic stimulation.[19] Indeed, RUNX2 expression is seen to intensify on these surfaces and is noted to be present in the cytoplasm as well as the nuclei. This perhaps suggests shuttling into the cytoplasm to allow phosphorylation and activation. It is thus logical that these particular topographies go on to induce the highest levels of OPN and OC expression. The 220-nm-deep features were particularly

potent at initiating the deposition of these mature osteoblast markers (OC is totally exclusive to maturing osteoblasts).

We have demonstrated induction of osteogenesis in a cell population that is a suitable model for the cell mix present around joint replacements. Nanopits (220-nm deep) with a diameter of 30 μm had the greatest inductive potential. This would be a suitable nanopattern to develop using implantable orthopaedic materials, such as metals and ceramics, and continued use for further in vitro experimentation. There has been great interest in the development of such modified surfaces and materials with scope for a wide range of future orthopaedic applications.[33,34] The expanding body of evidence and research exploring the use of nanotechnology in orthopaedic surgery may herald a new generation of implants and material.

Supplementary Information

Fabrication of nickel shims

Silicon wafers (Compart Technologies, UK) were cleaned under acetone in an ultrasonic bath for 5 min. They were rinsed thoroughly in reverse osmosis water (ROH$_2$O) (29) and blow dried with an air gun. Next, they were spun with primer (Shipley AZ Coupler, Shipley, UK) for 30 s at 4000 r/min, then spun with S1818 photoresist (Shipley AZ Coupler) for 30 s at 4000 r/min and baked for 30 min at 90°C. The resulting layer was measured to be 1.8 μm thick. The photoresist layer was exposed to UV light through a chrome mask on a Karl Suss MA6 mask aligner for 3.8 s. Then, the resist layer was developed for 75 s in 50:50, Microposit developer (Shipley AZ Coupler):ROH$_2$O.

The developed circle patterns were then used as a mask for reactive ion etching. The silicon substrate was etched in the silicon tetrachloride gas plasma of a Plasmalab System 100 machine (gas flow = 18 sccm, pressure = 9 mTorr, rf power = 250 W, DC bias = −300 V). Each wafer was etched individually at 18 min at a nominal etch rate of 18 nm/min. All wafers were stripped of resist in an acetone ultrasound bath for 5 min, followed by a 5-min soak in concentrated sulphuric acid/hydrogen peroxide mixture before rinsing in ROH$_2$O and drying in an air gun.

Nickel dies were made directly from the patterned resist samples. A thin (50 nm) layer of Ni-V was sputter coated on the samples. This layer acted as an electrode in the subsequent electroplating process. The dies were plated to a thickness of ca 300 μm. Once returned from the plater, the nickel shims were cleaned by first stripping the protective polyurethane coating using chloroform in an ultrasound bath for 10–15 min. Second, silicon residue was stripped by being wet etched in 25% potassium hydroxide at 80°C for 1 h. Shims were rinsed thoroughly in ROH$_2$O and then

air gun dried. The shims were finally trimmed to approximately 30 mm × 30 mm sizes using a metal guillotine.

Declaration of conflicting interests

The author(s) declared the following potential conflicts of interest with respect to the research, authorship, and/or publication of this article: Each author certifies that he or she has no commercial associations that might pose a conflict of interest in connection with the submitted article.

References

1. Biggs MJ, Richards RG, McFarlane S, et al. Adhesion formation of primary human osteoblasts and the functional response of mesenchymal stem cells to 330 nm deep microgrooves. *J R Soc Interface* 2008; 5(27): 1231–1242.
2. Dalby MJ, McCloy D, Robertson M, et al. Osteoprogenitor response to semi-ordered and random nanotopographies. *Biomaterials* 2006; 27: 2980–2987.
3. Kay S, Thapa A, Haberstroh KM, et al. Nanostructured polymer/nanophase ceramic composites enhance osteoblast and chondrocyte adhesion. *Tissue Eng* 2002; 8: 753–761.
4. Sjöström T, Dalby MJ, Hart A, et al. Fabrication of pillar-like titania nanostructures on titanium and their interactions with human skeletal stem cells. *Acta Biomater* 2009; 5(5): 1433–1441.
5. Webster TJ and Ejiofor JU. Increased osteoblast adhesion on nanophase metals: Ti, Ti6Al4V, and CoCrMo. *Biomaterials* 2004; 25: 2731–2739.
6. Webster TJ, Seigel RW and Bizios R. Osteoblast adhesion on nanophase ceramics. *Biomaterials* 1999; 20(13): 1221–1227.
7. Wilkinson A, Hewitt RN, McNamara LE, et al. Biomimetic microtopography to enhance osteogenesis in vitro. *Acta Biomater* 2011; 7(7): 2919–2925.
8. Andersson AS, Bäckhed F, von Euler A, et al. Nanoscale features influence epithelial cell morphology and cytokine production. *Biomaterials* 2003; 24: 3427–3436.
9. Andersson AS, Olsson P, Lidberg U, et al. The effects of continuous and discontinuous groove edges on cell shape and alignment. *Exp Cell Res* 2003; 288(1): 177–188.
10. Dalby MJ, McCloy D, Robertson M, et al. Osteoprogenitor response to defined topographies with nanoscale depths. *Biomaterials* 2006; 27: 1306–1315.
11. De Oliveira PT and Nanci A. Nanotexturing of titanium-based surfaces upregulates expression of bone sialoprotein and osteopontin by cultured osteogenic cells. *Biomaterials* 2004; 25: 403–413.
12. Lamers E, Walboomers XF, Domanski M, et al. The influence of nanoscale grooved substrates on osteoblast behavior and extracellular matrix deposition. *Biomaterials* 2010; 31: 3307–3316.
13. Dalby MJ, Gadegaard N, Tare R, et al. The control of human mesenchymal cell differentiation using nanoscale symmetry and disorder. *Nat Mater* 2007; 6(12): 997–1003.
14. McNamara LE, McMurray RJ, Biggs MJP, et al. Nanotopographical control of stem cell differentiation. *J Tissue Eng* 2010; 2010: 120623.
15. Engh CA, Bobyn JD and Glassman AH. Porous-coated hip replacement. The factors governing bone ingrowth, stress shielding, and clinical results. *J Bone Joint Surg Br* 1987; 69(1): 45–55.
16. Mata A, Hsu L, Capito R, et al. Micropatterning of bioactive self-assembling gels. *Soft Matter* 2009; 5(6): 1228–1236.
17. Biggs MJ, Richards RG, Gadegaard N, et al. The use of nanoscale topography to modulate the dynamics of adhesion formation in primary osteoblasts and ERK/MAPK signalling in STRO-1+ enriched skeletal stem cells. *Biomaterials* 2009; 30: 5094–5103.
18. Engler AJ, Sen S, Sweeney HL, et al. Matrix elasticity directs stem cell lineage specification. *Cell* 2006; 126: 677–689.
19. Kilian KA, Bugarija B, Lahn BT, et al. Geometric cues for directing the differentiation of mesenchymal stem cells. *Proc Natl Acad Sci U S A* 2010; 107: 4872–4877.
20. McBeath R, Pirone DM, Nelson CM, et al. Cell shape, cytoskeletal tension, and RhoA regulate stem cell lineage commitment. *Dev Cell* 2004; 6: 483–495.
21. McMurray RJ, Gadegaard N, Tsimbouri PM, et al. Nanoscale surfaces for the long-term maintenance of mesenchymal stem cell phenotype and multipotency. *Nat Mater* 2011; 10: 637–644.
22. Tsimbouri PM, McMurray RJ, Burgess KV, et al. Using nanotopography and metabolomics to identify biochemical effectors of multipotency. *ACS Nano* 2012; 6(11): 10239–10249.
23. Ge C, Xiao G, Jiang D, et al. Critical role of the extracellular signal-regulated kinase-MAPK pathway in osteoblast differentiation and skeletal development. *J Cell Biol* 2007; 176: 709–718.
24. Hamamura K, Jiang C and Yokota H. ECM-dependent mRNA expression profiles and phosphorylation patterns of p130Cas, FAK, ERK and p38 MAPK of osteoblast-like cells. *Cell Biol Int* 2010; 34: 1005–1012.
25. Hamilton DW and Brunette DM. The effect of substratum topography on osteoblast adhesion mediated signal transduction and phosphorylation. *Biomaterials* 2007; 28: 1806–1819.
26. Xiao G, Jiang D, Gopalakrishnan R, et al. Fibroblast growth factor 2 induction of the osteocalcin gene requires MAPK activity and phosphorylation of the osteoblast transcription factor, Cbfa1/Runx2. *J Biol Chem* 2002; 277: 36181–36187.
27. Veyrat-Masson R, Boiret-Dupré N, Rapatel C, et al. Mesenchymal content of fresh bone marrow: a proposed

quality control method for cell therapy. *Br J Haematol* 2007; 139(2): 312–320.

28. Liao H, Andersson AS, Sutherland D, et al. Response of rat osteoblast-like cells to microstructured model surfaces in vitro. *Biomaterials* 2003; 24(4): 649–654.

29. Bettinger CJ, Langer R and Borenstein JT. Engineering substrate topography at the micro- and nanoscale to control cell function. *Angew Chem Int Ed Engl* 2009; 48(30): 5406–5415.

30. Lim JY, Dreiss AD, Zhou Z, et al. The regulation of integrin-mediated osteoblast focal adhesion and focal adhesion kinase expression by nanoscale topography. *Biomaterials* 2007; 28: 1787–1797.

31. Loesberg WA, TeRiet J, Van Delft FC, et al. The threshold at which substrate nanogroove dimensions may influence fibroblast alignment and adhesion. *Biomaterials* 2007; 28(27): 3944–3951.

32. McNamara LE, Sjöström T, Seunarine K, et al. Investigation of the limits of nanoscale filopodial interactions. *J Tissue Eng* 2014; 5: 2041731414536177.

33. Sullivan MP, McHale KJ, Parvizi J, et al. Nanotechnology: current concepts in orthopaedic surgery and future directions. *Bone Joint J* 2014; 96(5): 569–573.

34. Tasker LH, Sparey-Taylor GJ and Nokes LD. Applications of nanotechnology in orthopaedics. *Clin Orthop Relat Res* 2007; 456: 243–249.